Double-Decker Coordination Cages

Article *in* Berichte der deutschen chemischen Gesellschaft · April 2016

DOI: 10.1002/ejic.201600259

CITATIONS
16

READS
224

6 authors, including:

Sreenivasulu Bandi
Indian Institute of Technology Madras
8 PUBLICATIONS **126** CITATIONS
SEE PROFILE

Sagarika Samantray
Indian Institute of Technology Madras
3 PUBLICATIONS **44** CITATIONS
SEE PROFILE

Deepan Chakravarthy
Indian Institute of Technology Madras
18 PUBLICATIONS **254** CITATIONS
SEE PROFILE

Amlan Kumar Pal
Indian Institute of Technology Jammu
57 PUBLICATIONS **955** CITATIONS
SEE PROFILE

ChemPubSoc Europe

DOI: 10.1002/ejic.201600259

EurJIC European Journal of Inorganic Chemistry

Full Paper

Cage Compounds

Double-Decker Coordination Cages

Sreenivasulu Bandi,[a] Sagarika Samantray,[a] Rajan Deepan Chakravarthy,[a] Amlan K. Pal,[b] Garry S. Hanan,*[b] and Dillip Kumar Chand*[a]

Abstract: Bis(pyridin-3-ylmethyl) pyridine-3,5-dicarboxylate (**L**) possessing one internal and two terminal pyridine moieties displayed differential coordination ability when combined with suitable Pd^{II} components. The compound **L** acted as a bidentate chelating ligand to form mononuclear complexes when combined with *cis*-[Pd(tmeda)$(NO_3)_2$] or $Pd(NO_3)_2$ in calculated ratios. The combination of $Pd(NO_3)_2$ with **L** in a ratio of 3:4, however, afforded the trinuclear "double-decker" cage $[(NO_3)_2{\subset}Pd_3(\mathbf{L})_4](NO_3)_4$, in which **L** acts as a nonchelating tridentate ligand and the counter anion (i.e., NO_3^-) acts as template. The encapsulated NO_3^- can be replaced by F^-, Cl^-, or Br^- but not by I^-. The F^--encapsulated cage could not be isolated due to its reactivity, whereas the Cl^- or Br^- encapsulated cages could be isolated. Although anionic guests such as NO_3^-, Cl^-, or Br^- stabilized the cages, the presence of excess Cl^- or Br^- (not NO_3^-) facilitated decomplexation reactions releasing the ligand. The complexation of $Pd(Y)_2$ (Y = BF_4^-, PF_6^-, $CF_3SO_3^-$, or ClO_4^-) with **L** afforded the corresponding mononuclear complexes under appropriate conditions. However, these counter anions could not act as templates for the construction of double-decker cages.

Introduction

The concept of self-assembly governs a variety of phenomena in objects ranging from nanosized assemblies to the universe.[1] We are interested in the synthesis and reactivity of Pd^{II}-based self-assembled discrete coordination complexes.[2] The design and synthesis of coordination cage molecules using a variety of metal and ligand components is an alternative and convenient approach to the preparation of large-sized supramolecular hosts.[3,4] Understanding the emergent behaviors of certain self-assembled coordination complexes[5] has been a very recent trend in supramolecular chemistry.

In a preliminary communication we recently reported on stoichiometrically controlled and revocable self-assembled "spiro" and quadruple-stranded "double-decker"-type coordination cages.[6] The molecular architectures of the "spiro"- and "double-decker"-type assemblies could be classified, on the basis of their compositions, into $Pd_1\mathbf{L}_2$ and $Pd_3\mathbf{L}_4$ structures, respectively. In this paper we disclose a detailed investigation of the said double-decker cages and a few related compounds. The nature and stoichiometry of the Pd^{II} components and the role of the counter anion have been found to be crucial for the formation of the cages.

The first designed and synthesized $Pd_2\mathbf{L}_4$-type coordination cage molecule was reported by McMorran and Steel[7] in 1998. Subsequently, a large number of $Pd_2\mathbf{L}_4$-type cages have been prepared, studied, and reviewed.[8,9] The architecture of a $Pd_3\mathbf{L}_4$-type double-decker coordination cage was also originally conceived by McMorran and Steel[10] in 2002, however, they could not realize their design, probably due to limitations in ligand design. In 2014 we successfully demonstrated the construction of this long-awaited architecture by using a newly designed ligand and named the self-assembled $Pd_3\mathbf{L}_4$-type coordination complex a "double-decker" cage (Figure 1).[6] In addition, Clever and co-workers utilized a rigid tridentate ligand for the construction of an elegant $Pd_3\mathbf{L}_4$-type double-decker in 2015.[11]

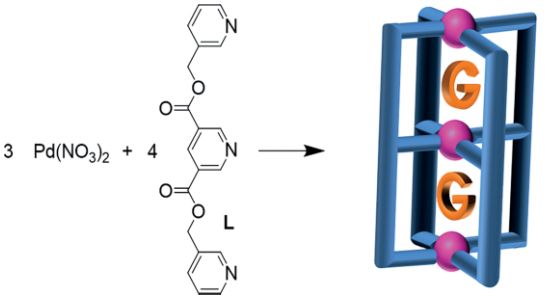

Figure 1. Cartoon representation of the guest-induced "double-decker" coordination cage $[(G)_2{\subset}Pd_3\mathbf{L}_4]^{4+}$. In this case G represents NO_3^-.

Complexation reactions of the ligand **L** were carried out with the *cis*-protected Pd^{II} complex, that is, *cis*-[Pd(tmeda)$(NO_3)_2$] and a simple Pd^{II} salt, that is, $Pd(NO_3)_2$. The complexation behaviors displayed by both types of metal components were found to be comparable as well as contrasting depending upon the stoichiometry of the metal and ligand. Stoichiometrically con-

[a] *Department of Chemistry, Indian Institute of Technology Madras, Chennai 600036, India*
E-mail: dillip@iitm.ac.in
http://chem.iitm.ac.in/faculty/dillipkumarchand/
[b] *Department of Chemistry, University of Montreal, Montreal, Canada*
E-mail: garry.hanan@umontreal.ca
http://en.chimie.umontreal.ca/department-directory/vue/hanan-garry/
Supporting information for this article is available on the WWW under http://dx.doi.org/10.1002/ejic.201600259.

trolled complexation behavior in supramolecular coordination chemistry has not been extensively explored,[6,12] which we have sought to address in this work. The coordination chemistry and anion-binding properties of a double-decker-type cage with the composition Pd_3L_4 is the major focus of this paper. The anion-binding properties and nature of the Pd_3L_4 cage molecules have been found to be synergic in nature.

Results and Discussion

Design and Synthesis of Ligand L

The tridentate nonchelating ligand bis(pyridin-3-ylmethyl) pyridine-3,5-dicarboxylate (**L**, Scheme 1) was prepared by the condensation of freshly prepared pyridine-3,5-dicarbonyl chloride hydrochloride with 3-hydroxymethylpyridine in dry dichloromethane in the presence of triethylamine. The reaction mixture was stirred at room temperature for 24 h followed by aqueous workup and column chromatographic purification to afford ligand **L** as a white solid that was well characterized (see Figures S1–S5 in the Supporting Information).

The design and possible coordination modes of the ligand **L** are deliberated here. Ligand **L** has three pyridine moieties as donor sites crafted in the ligand strand. Two of these pyridines are terminal and symmetrically disposed with respect to the central/internal pyridine. The internal pyridine ring is substituted by two electron-withdrawing groups located at the 3- and 5-positions of the ring. The nature of the spacer units, that is, $-C(O)OCH_2-$, is such that the ligand is neither completely rigid nor flexible. The three coordination vectors of the semi-rigid (or semi-flexible) ligand are expected to be randomly oriented, but they could also be unidirectional and parallel to each other in one of the conformations of **L**. This would happen only if the coordination vectors are reoriented, particularly during the process of complexation with suitable metal ions. Such a process could be driven by the thermodynamic stability of the ensuing self-assembled complex. Thus, a given strand of the ligand should coordinate with three different metal centers through the three pyridine nitrogen centers. Both of the terminal coordination vectors are also capable of converging towards a single metal center, due to the semi-flexible nature of the spacer, to create a large chelate ring (Scheme 1). It is more appropriate to term such a ring as a metallo-macrocycle. The ligand showed differential coordination ability[12,13] under appropriate conditions and acted either as a bi- or tridentate ligand in a stoichiometrically controlled manner upon complexation with a calculated amount of $Pd(NO_3)_2$ (see Scheme 2).

Complexation of *cis*-[Pd(tmeda)$(NO_3)_2$] with the Ligand L

A family of $[Pd_x(tmeda)_xL_y]$-type self-assembled compounds have been prepared by the complexation of *cis*-[Pd(tmeda)$(NO_3)_2$] with selected mono/polydentate ligands under suitable reaction conditions.[4a] We have studied the complexation behavior of *cis*-[Pd(tmeda)$(NO_3)_2$] with the tridentate ligand **L** (Scheme 1). In view of the possibility of differential coordination of the ligand, the complexation reactions were performed at two different ratios of metal component to ligand.

The reaction of *cis*-[Pd(tmeda)$(NO_3)_2$] with **L** in a ratio of 1:1 is a suitable stoichiometry for the preparation of a mononuclear

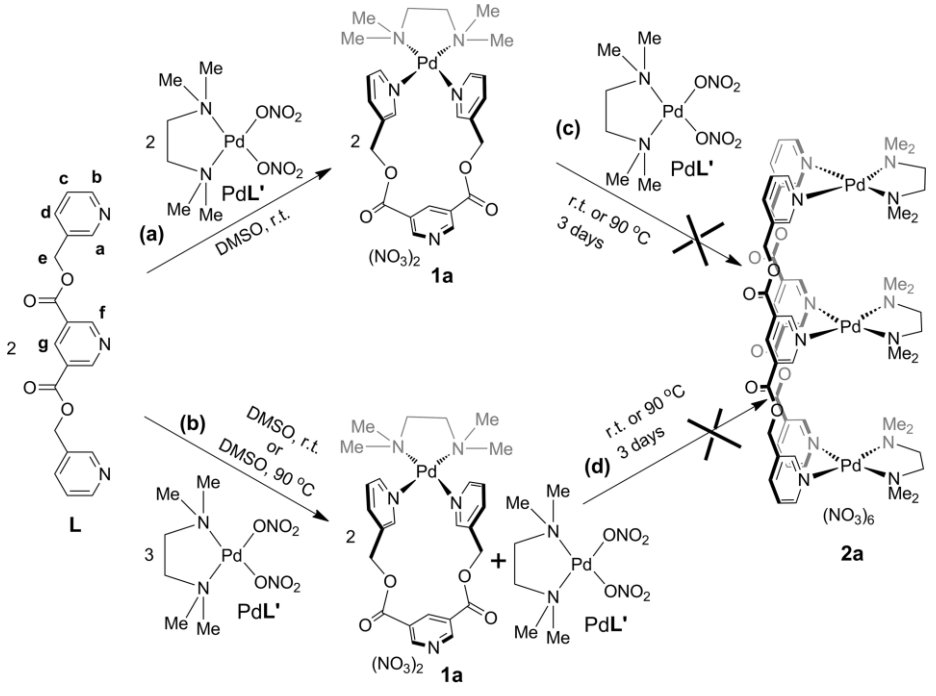

Scheme 1. Complexation of *cis*-[Pd(tmeda)$(NO_3)_2$] with the ligand **L** in ratios of (a) 1:1 and (b) 3:2. The mononuclear complex [Pd(tmeda)(**L**)]$(NO_3)_2$ (**1a**) was formed under both conditions as the exclusive self-assembled product. (c,d) Trinuclear $[Pd_3(tmeda)_3(L)_2](NO_3)_6$ (**2a**) was not formed even at elevated temperatures.

self-assembled complex[14] with a large chelate ring. In the mononuclear complex, the terminal pyridine nitrogen lone pairs are expected to participate in metal–ligand bond formation. The ligand could potentially display tridentate nonchelating behavior when the ratio of *cis*-[Pd(tmeda)$(NO_3)_2$] to **L** is 3:2, to yield the target "double-saddle"-type[3] trinuclear assembly of composition $Pd_3(tmeda)_3\mathbf{L}_2$.

The reaction of *cis*-[Pd(tmeda)$(NO_3)_2$] and **L** in a ratio of 1:1 resulted in the mononuclear complex [Pd(tmeda)(**L**)]$(NO_3)_2$ (**1a**; Scheme 1, a). The isolated complex **1a** was characterized by NMR spectroscopy (Figure 2 and Figures S6 and S7 in the Supporting Information), MS (Figure S8), and single-crystal XRD (Figure 3). The ^{1}H NMR spectrum of **1a** recorded in [D_6]DMSO shows a single set of peaks supporting the exclusive formation of a discrete complex. The signals of the terminal pyridine α-H atoms are significantly shifted downfield ($\Delta\delta$ = 0.87 and 0.73 ppm for H_a and H_b, respectively) compared with the free ligand **L**, thereby confirming the formation of a metal–ligand bond (Figure 2). Furthermore, the insignificant change ($\Delta\delta$ = 0.04 ppm) in the position of the signal due to H_f indicates the nonparticipation of the internal pyridine in the complex. This observation supports the bidentate nature of the ligand in its bonded form in complex **1a**. Incidentally, the methylene protons (i.e., H_e) appear as a pair of doublets and hence the two protons of a given methylene group are diastereotopic in the bound form of the ligand, which indicates some restriction in the rotation of the pyridine rings.

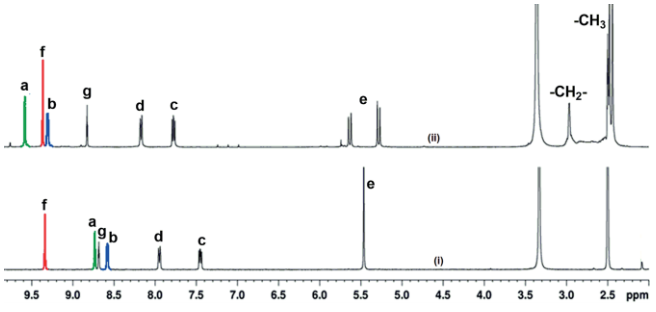

Figure 2. ^{1}H NMR (400 MHz) spectra of (i) ligand **L** and (ii) [Pd(tmeda)(**L**)]$(NO_3)_2$ (**1a**) in [D_6]DMSO.

The composition of **1a** was supported by MS (see Figure S8); the mass spectrum shows a prominent isotopic peak pattern at m/z = 285.52 for the dication $[\mathbf{1a} - 2NO_3]^{2+}$, which corresponds to the loss of two NO_3^- ions from the title mononuclear compound. The isotopic pattern confirms the presence of one palladium in the dication. The experimental pattern is similar to that calculated.

However, for a 3:2 ratio of *cis*-[Pd(tmeda)$(NO_3)_2$] to **L** (Scheme 1, b), the probable trinuclear complex $[Pd_3(tmeda)_3(\mathbf{L})_2](NO_3)_6$ (**2a**) was not formed. Instead, the mononuclear complex **1a** was isolated from the reaction mixture. The ^{1}H NMR spectrum of the isolated product is comparable to that of complex **1a** prepared with a 1:1 ratio of the reactants. The reaction with a 3:2 ratio was therefore followed in situ by performing the reaction in [D_6]DMSO; the signals in the ^{1}H NMR spectra confirmed the formation of **1a** as the exclusive product and the presence of unreacted *cis*-[Pd(tmeda)$(NO_3)_2$] (Scheme 1, b and Figures S9 in the Supporting Information). The reaction conditions were further varied by changing the temperature and solvent; however, our efforts to prepare the trinuclear complex were not successful. The reaction did not proceed beyond the mononuclear architecture when stirred at elevated temperature such as 90 °C in [D_6]DMSO for a period as long as 3 days (Scheme 1 c, d). The reaction of *cis*-[Pd(tmeda)$(Y)_2$] (Y = NO_3^-, BF_4^-, PF_6^-, $CF_3SO_3^-$, or ClO_4^-) with **L** produced comparable results (see Scheme S1a).

The reaction to yield the trinuclear complex **2a** was studied in the gaseous state by using the Gaussian 09 software package.[15] The geometries of the reactant and product molecules were optimized and their frequencies were calculated at the B3LYP/6-31G* level of theory. The overall Gibbs free energy (ΔG) and enthalpy (ΔH) for the formation of the trinuclear complex $[Pd_3(tmeda)_3(\mathbf{L})_2]^{6+}$ by the reaction of 1 equiv. of $[Pd(tmeda)]^{2+}$ and 2 equiv. of $[Pd(tmeda)(\mathbf{L})]^{2+}$ were found to be infeasible (+240.339 kcal mol^{-1}) and endothermic (+210.693 kcal mol^{-1}), respectively (see Figure S61 and Table S3).

Crystal Structure of [Pd(tmeda)(L)]$(NO_3)_2$ (1a)

Single crystals of **1a** suitable for XRD data collection were grown by the slow diffusion of ethyl acetate into a DMSO solution of **1a**. The crystal structure (Figure 3, a and Table S4 in the Supporting Information) shows one ligand **L** coordinated to two sites of the *cis*-protected Pd^{II} ion forming a molecular loop-like arrangement. The calculated Pd–N bond lengths in the complex are in the range 2.03(2)–2.07(3) Å and the *cis*-N–Pd–N bond angles span the range 86.44(13)–92.71(11)°.

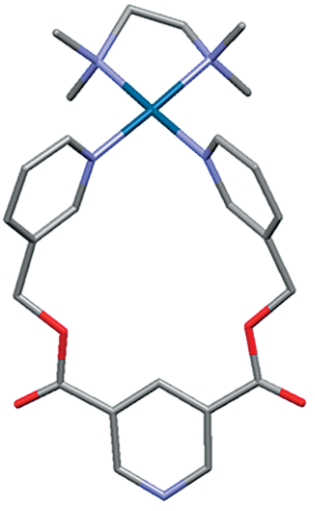

Figure 3. Crystal structure of [Pd(tmeda)(**L**)]$(NO_3)_2$ (**1a**). The counter anions and solvent molecules have been omitted for clarity.

The packing arrangement of the cation of **1a** is shown in Figure S63. It displays a one-dimensional molecular-pillar-like arrangement formed through weak supramolecular interactions.[3,16]

Complexation of $Pd(NO_3)_2$ with the Ligand L

A family of $Pd_m\mathbf{L}_n$-type self-assembled complexes have been prepared by the complexation of Pd^{II} with selected mono/poly-

dentate ligands under suitable reaction conditions.[4a] In this work, the stoichiometry of metal to ligand was varied to study the differential coordination ability of the ligand **L**. Thus, the reaction of $Pd(NO_3)_2$ with the ligand **L** was performed in ratios of 1:2 and 3:4 (Scheme 2). It is crucial to mention here that the sample of $Pd(NO_3)_2$ used for the complexation reactions was acquired from a commercial source (relevant to the discussion in later sections).

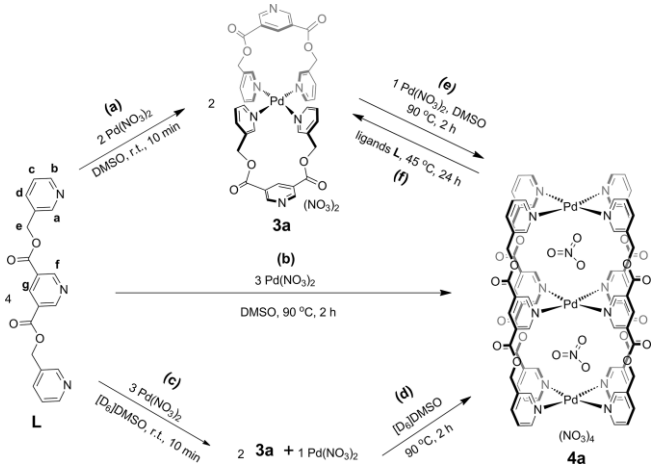

Scheme 2. Complexation of $Pd(NO_3)_2$ with the ligand **L** at specific metal to ligand ratios and temperatures showing the exclusive formation of the "spiro"-type mononuclear complex $[Pd(\mathbf{L})_2](NO_3)_2$ (**3a**) and "double-decker"-type trinuclear complex $[(NO_3)_2{\subset}Pd_3(\mathbf{L})_4](NO_3)_4$ (**4a**). Complexes **3a** and **4a** are interconvertible under appropriate conditions. Note: In step (f), 2 equiv. of **L** are added to 1 equiv. of **4a** to afford 3 equiv. of **3a**.

All the reactions were carried out in either DMSO or $[D_6]$DMSO for isolation and monitoring purposes, respectively. The precipitation method was used to isolate the desired products, through the addition of excess EtOAc. Although the "spiro"-type[14] mononuclear product $[Pd(\mathbf{L})_2](NO_3)_2$ (**3a**) was isolated from the reaction carried out with a 1:2 ratio of metal to ligand (Scheme 2, a), the "double-decker"-type trinuclear product $[Pd_3(\mathbf{L})_4](NO_3)_6$ (**4a**) was formed with a 3:4 ratio of the reagents (Scheme 2, b). Thus, in this latter case the internal pyridine participates in the reaction of **L** with $Pd(NO_3)_2$ to give the very symmetrical double-decker cage-like architecture **4a** (Scheme 2). A detailed investigation disclosed in the present work satisfactorily accounts for the synergic role of NO_3^- as well as the ensuing three-dimensional cavity that facilitates the formation of "double-decker" **4a**. This result is in sharp contrast to the complexation behavior of *cis*-$[Pd(tmeda)(NO_3)_2]$ with the ligand **L**, when the geometrically probable complex **2a** could not be formed (Scheme 1, b–d). The internal pyridine nitrogen of **L** is probably situated in a disadvantageous position for coordination with a metal center. The complexation of *cis*-$[Pd(tmeda)(NO_3)_2]$ with **L** proved unsuitable for the synthesis of **2a** (Scheme 1) and the internal pyridine is not utilized.

We have acquired enough evidence to propose the chemical formula of the trinuclear complex **4a** as the inclusion complex $[(NO_3)_2{\subset}Pd_3(\mathbf{L})_4](NO_3)_4$ instead of $[Pd_3(\mathbf{L})_4](NO_3)_6$. This formulation emphasizes the encapsulation/templating role of the two NO_3^- counter anions, as clarified in later sections. In particular, the choice of counter anion (NO_3^- or other anions) and the method of preparation of the Pd^{II} salt immensely influenced the coordination chemistry of the system under investigation.

The ^1H NMR spectrum of the isolated self-assembled mononuclear complex $[Pd(\mathbf{L})_2](NO_3)_2$ (**3a**) was recorded in $[D_6]$DMSO and shows a single set of peaks supporting the exclusive formation of a discrete complex. The signals of terminal pyridine α-H atoms are significantly shifted downfield ($\Delta\delta$ = 0.94 and 0.81 ppm for H_a and H_b, respectively) as compared with the free ligand **L**, which confirms the formation of the metal–ligand bond (Figure 4 and Figure S10 in the Supporting Information). Furthermore, an insignificant change in the position of the signal due to H_f is observed ($\Delta\delta$ = 0.05 ppm), which indicates the nonparticipation of the internal pyridine in the complexation reaction. This observation supports the bidentate nature of the ligand in its bound form in complex **3a**. The signal of the methylene protons (i.e., H_e) in **3a** appears as a singlet in contrast to the doublet of doublets observed for **1a**. This indicates faster rotation of the pyridine rings and Pd–**L** exchange in **3a**. The ^1H NMR spectrum of the isolated complex **4a** (Figure 4 and Figure S13), which is best represented as $[(NO_3)_2{\subset}Pd_3(\mathbf{L})_4](NO_3)_4$, shows evidence for a tridentate binding mode of the bound ligand. Although signals of H_a and H_b are shifted downfield ($\Delta\delta$ = 1.16, and 0.65 ppm for H_a and H_b, respectively) compared with in the free ligand, the signal of H_f is also considerably shifted downfield ($\Delta\delta$ = 1.30 ppm), which confirms the participation of the internal pyridine in the complexation reaction.

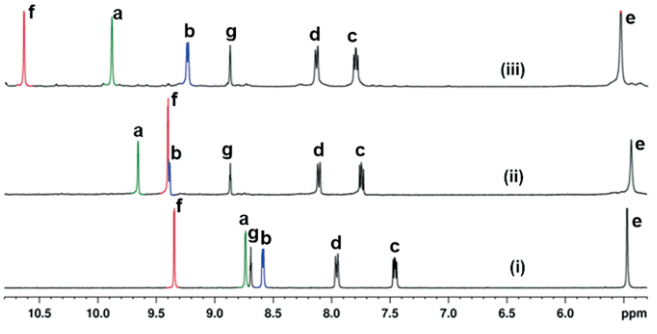

Figure 4. ^1H NMR (400 MHz) spectra in $[D_6]$DMSO of (i) ligand **L**, (ii) "spiro"-type $[Pd(\mathbf{L})_2](NO_3)_2$ (**3a**), and (iii) "double-decker"-type $[(NO_3)_2{\subset}Pd_3(\mathbf{L})_4](NO_3)_4$ (**4a**).

The "spiro"-type mononuclear complex $[Pd(\mathbf{L})_2](NO_3)_2$ (**3a**) was spontaneously assembled at room temperature within 10 min when commercially available $Pd(NO_3)_2$ was combined with **L** in a ratio of either 1:2 (Scheme 2, a, Figure 4, and Figure S10) or 3:4 (Scheme 2, c and Figure S16) in $[D_6]$DMSO. In the former ratio (1:2), only the mononuclear complex **3a** was formed (Scheme 2, a). However, in the latter case (3:4), presumably unreacted $Pd(NO_3)_2$ remained in the solution along with **3a** (Scheme 2, c).

Subsequent addition of the required amount of $Pd(NO_3)_2$ to the former solution of **3a** followed by heating at 90 °C (Scheme 2, e and Figure S17) facilitated the formation of the thermodynamically stable trinuclear "double-decker"-type product **4a**. In the latter case, the required amount of $Pd(NO_3)_2$

was already present in solution, which favored the spontaneous reorganization of complex **3a** upon heating at 90 °C to form complex **4a** (Scheme 2, d and Figure S16). Therefore, compound **3a** could be considered as an intermediate complex. Because complex **3a** could be detected in the preparation of **4a**, it is proposed that complex **3a** is a kinetically controlled product in the presence of excess $Pd(NO_3)_2$. However, the isolated complex **3a** was found to be stable in the absence of additional $Pd(NO_3)_2$; it could be stored both in the solid and solution states without further reorganization. A solution of **3a** in [D_6]DMSO was heated at 90 °C and no changes were observed (see Figures S19 and S44).

As discussed above, the formation of complexes **3a** and **4a** was found to be controlled by the stoichiometry of the metal and ligand components. Both of these stoichiometrically controlled complexes were also found to be revocable, through dynamic processes, upon subjecting them to appropriate conditions (Scheme 2, e, f). The reaction of 2 equiv. of **3a** with 1 equiv. of $Pd(NO_3)_2$ could produce complex **4a** quantitatively (see Figure S17). Similarly, the reaction of **4a** with 2 equiv. of ligand **L** produced complex **3a** (see Figure S18). The revocable nature of the complexes was studied by DFT calculations using the Gaussian 09 software package.[15] The results are presented in Table S3 and a brief discussion is also provided there.

The compositions of **3a** and **4a** were further evidenced by MS (ESI) and the structures of $[Pd(\mathbf{L})_2](NO_3)_2$ (**3a**) and $[Pd(\mathbf{L})_2](BF_4)_2$ (**3b**) were confirmed by single-crystal X-ray diffraction (see Figure 6). The MS (ESI) of compound **3a** (see Figure S12) shows a prominent peak at m/z = 402.05 corresponding to the dication $[\mathbf{3a} - 2NO_3]^{2+}$ formed by the loss of two NO_3^- ions. The isotopic pattern confirms the presence of one unit of palladium and is in good agreement with the calculated data. The MS (ESI) of compound **4a** (see Figure S15) shows peaks at m/z = 982.73, 634.35, and 460.23, which correspond to the cations $[\mathbf{4a} - 2NO_3]^{2+}$, $[\mathbf{4a} - 3NO_3]^{3+}$, and $[\mathbf{4a} - 4NO_3]^{4+}$ formed by the loss of two, three, and four NO_3^- ions, respectively. The isotopic patterns of fragments containing three palladium units are in good agreement with the calculated data.

Complexation of $Pd(NO_3)_2$ (Prepared from $PdCl_2$ and $AgNO_3$) with the Ligand L

Stock solutions of $Pd(NO_3)_2$ were prepared separately in DMSO and [D_6]DMSO by treating $PdCl_2$ with $AgNO_3$ and then allowing the solution to stand to allow the precipitated AgCl to settle. Complexation reactions of the as-prepared $Pd(NO_3)_2$ (in [D_6]DMSO) with the ligand **L** were carried out in ratios of 1:2 and 3:4 of metal to ligand, targeting the complexes $[Pd(\mathbf{L})_2](NO_3)_2$ (**3a**) and $[(NO_3)_2{\subset}Pd_3(\mathbf{L})_4](NO_3)_4$ (**4a**), respectively. However, as confirmed by the ^{1}H NMR spectra of the samples, a mixture of products, including the targeted compounds, was formed for each ratio. For the 1:2 ratio of metal to ligand, although the expected complex **3a** was found to be the major product (see Scheme S20 and Figure S51 in the Supporting Information), it was not the exclusive product, whereas, for a ratio of 3:4, complex **4a** was found, surprisingly, to be only a minor product (see Scheme S22 and Figure S53).

It was suspected, and later confirmed, that the presence of small amounts of residual AgCl in solution was responsible for the formation of the mixture of products. Thus, the solution of $Pd(NO_3)_2$ was centrifuged to effectively settle the precipitated AgCl and the solution was separated by using a syringe. This process of centrifugation and separation of the $Pd(NO_3)_2$ solution was repeated until no AgCl sedimentation was visible to the naked eye (four cycles). The purified $Pd(NO_3)_2$ was then used for complexation reactions with the ligand **L**. To our satisfaction, the targeted complex **3a** was found to be an almost exclusive product for a 1:2 ratio of metal to ligand (see Scheme S21 and Figure S52), whereas the targeted complex **4a** was found to be the major product (see Scheme S23 and Figure S54) although not exclusive for the 3:4 ratio of metal to ligand.

To determine whether Ag^I or Cl^- or both the ions are responsible for the formation of the mixture of products, the following experiments were performed. The complexation of "commercially available" $Pd(NO_3)_2$ with the ligand **L** was carried out in the presence of deliberately added AgCl, $AgNO_3$, TBACl, or $TBANO_3$ (TBA = tetra-*n*-butylammonium). Although the presence of $AgNO_3$ or $TBANO_3$ did not alter the nature of the complexation, the presence of AgCl or TBACl produced a mixture of products in line with the influence of residual AgCl on the complexation reactions. Thus, it was concluded that Ag^I is an innocent spectator whereas Cl^- has a definite influence on the course of the complexation reactions studied here.

Halide-Encapsulated Double-Decker Cages

The NO_3^--encapsulated double-decker-type coordination cage $[(NO_3)_2{\subset}Pd_3(\mathbf{L})_4](NO_3)_4$ (**4a**) was considered suitable for the binding of appropriate anions in both of the cavities. In addition to the positive charges of the metal centers, the inner walls of the cavities are delineated with several electron-deficient pyridine α-H atoms, making the cavities suitable for binding electron-rich guests. It was envisaged that spherical halide ions could be encapsulated as guest molecules by combining **4a** with TBAX (X = F^-, Cl^-, Br^-, or I^-). In a typical experiment, a solution of TBAX in [D_6]DMSO was added portionwise to a solution of **4a** in [D_6]DMSO to monitor the progress of the reaction. The double-decker cage **4a** could exchange the encapsulated NO_3^- ions with two units of the incoming halide ions, one in each of the cavities (Scheme 3, Figure 5, and Figures S20–S40). Although F^-, Cl^-, and Br^- ions are accommodated, I^- ions could not enter the cavities. After a thorough investigation by ^{1}H NMR spectroscopy, it was understood that complexes of general formula $[(X)(NO_3){\subset}Pd_3(\mathbf{L})_4](NO_3)_4$ (X = F^-, Cl^-, or Br^-, corresponding to **5a**, **7a**, and **9a**) were initially formed along with other related cages (see Figures S20, S25, and S31). Subsequently, complexes of general formula $[(X)_2{\subset}Pd_3(\mathbf{L})_4](NO_3)_4$ (X = F^-, Cl^-, or Br^-, corresponding to **6a**, **8a**, and **10a**) were formed exclusively. The ^{1}H NMR spectra of **6a**, **8a**, and **10a** were recorded and compared

with that of **4a** (Figure 5). These complexes could also be prepared by alternative routes due to their dynamic behavior, as shown in Scheme 3, b, c (see also Figures S42 and S43). The binding of Cl^- in the cavity of a binuclear Pd_2L_4 cage has previously been reported by Puddephatt and co-workers.[17]

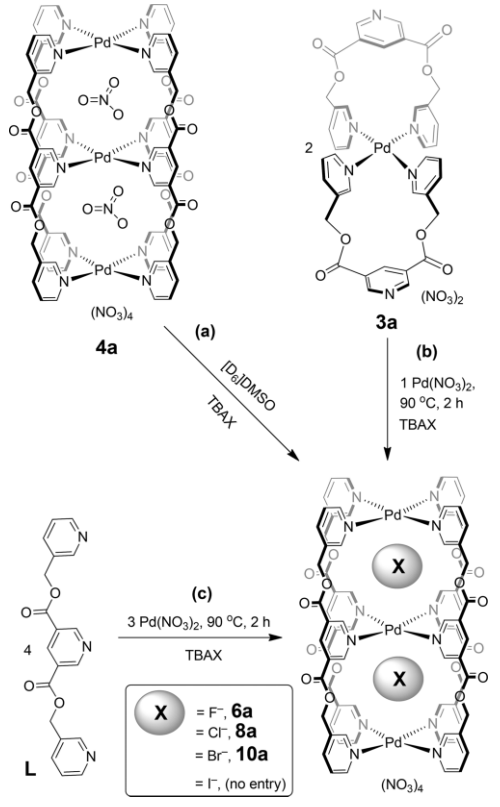

Scheme 3. Preparation of $[(X)_2{\subset}Pd_3(\mathbf{L})_4](NO_3)_4$ (**6a**, **8a**, and **10a**; X = F^-, Cl^-, or Br^-) by (a) encapsulation of two halide ions in the cage $[(NO_3)_2{\subset}Pd_3(\mathbf{L})_4](NO_3)_4$ (**4a**) by anion exchange or (b) the complexation of $Pd(NO_3)_2$ with $[Pd(\mathbf{L})_2](NO_3)_2$ (**3a**) in a 1:2 ratio in the presence of TBAX, or (c) the complexation of $Pd(NO_3)_2$ with **L** in a 3:4 ratio in the presence of TBAX. (TBAX = tetra-*n*-butylammonium halide, $n$$Bu_4NX$.).

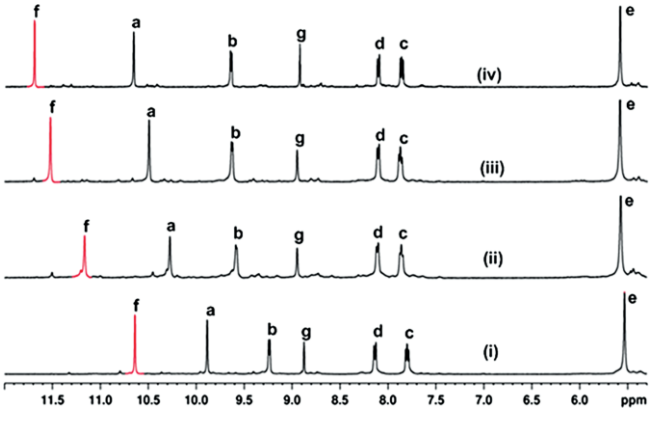

Figure 5. ^1H NMR (400 MHz) spectra in $[D_6]$DMSO for (i) $[(NO_3)_2{\subset}Pd_3(\mathbf{L})_4](NO_3)_4$ (**4a**), (ii) $[(F)_2{\subset}Pd_3(\mathbf{L})_4](NO_3)_4$ (**6a**), (iii) $[(Cl)_2{\subset}Pd_3(\mathbf{L})_4](NO_3)_4$ (**8a**), and (iv) $[(Br)_2{\subset}Pd_3(\mathbf{L})_4](NO_3)_4$ (**10a**).

Let us consider the case of Cl^- encapsulation. The portionwise addition of TBACl to a solution of **4a** resulted in the following situation. Initially, a mixture of $[(NO_3)_2{\subset}Pd_3(\mathbf{L})_4](NO_3)_4$ (**4a**), $[(Cl)(NO_3){\subset}Pd_3(\mathbf{L})_4](NO_3)_4$ (**7a**), and $[(Cl)_2{\subset}Pd_3(\mathbf{L})_4](NO_3)_4$ (**8a**) was observed that changes to a mixture of **7a** and **8a** and then exclusively to **8a** (see Figure S26). The addition of TBAF or TBABr to a solution of **4a** resulted in similar behavior, however, the addition of TBAI showed no changes in **4a** indicating no entry of I^- into the cavities (see Figures S21, S32, and S40).

The F^- encapsulated complex **6a** could neither be isolated in the pure state from its solution nor was stable in solution. A solution of **6a** underwent decomplexation, releasing the ligand within 1 day (see Figure S22). In contrast, complexes **8a** and **10a** could be isolated and were found to be stable enough. However, in the presence of an additional amount of TBACl (soluble Cl^-), complex **8a** was found to undergo decomplexation within 1 day, releasing the ligand **L**. Complex **10a** behaved similarly in the presence of an additional amount of TBABr (soluble Br^-). The strong interaction between Pd^{II} and F^- ions is probably responsible for the rapid decomposition of **6a**.

The intermediates formed during the halide encapsulation5 reactions are formulated as $[(X)(NO_3){\subset}Pd_3(\mathbf{L})_4](NO_3)_4$ (X = F^-, **5a**; Cl^-, **7a**; Br^-, **9a**). These intermediates are proposed on the basis of their ^1H NMR data. When the encapsulated guest moieties in the two cavities of the double-decker are the same, the ligand moieties should give one set of signals in the corresponding ^1H NMR spectrum. However, if the guests are different, the symmetry of the bound ligand is lost and two sets of signals are expected. The complexes $[(NO_3)_2{\subset}Pd_3(\mathbf{L})_4](NO_3)_4$ (**4a**) and $[(Cl)_2{\subset}Pd_3(\mathbf{L})_4](NO_3)_4$ (**8a**) each show one set of signals, whereas $[(Cl)(NO_3){\subset}Pd_3(\mathbf{L})_4](NO_3)$ (**7a**) exhibits two set of signals; the chemical shifts of one of the two sets of signals of **7a** were found to be close to those of **4a**, and the signals of the other set were found to be close to those of **8a**. The H_f atom clearly shows four signals for a mixture of **4a**, **7a**, and **8a** (see Figure S26). The chemical shifts of the signals of **5a**–**10a** (see Figures S21, S26, and S32) were compared with those of **4a** and found to be in line with expectation. The separation of peaks was noticed best for the encapsulation of Cl^-, as shown in Figure S26.

The formation of the complexes $[(X)_2{\subset}Pd_3(\mathbf{L})_4](NO_3)_4$ (X = Cl^-, **8a**; Br^-, **10a**) was confirmed from their MS (ESI) data. The single-crystal X-ray structures of $[(Cl)_2{\subset}Pd_3(\mathbf{L})_4](BF_4)_4$ (**8b**) and $[(Cl)_2{\subset}Pd_3(\mathbf{L})_4](PF_6)_4$ (**8c**) (Figure 7) further supported the claim. The MS (ESI) spectrum of compound **8a** (see Figure S30) shows peaks at m/z = 955.67, 616.13, and 446.58 corresponding to the cations $[\mathbf{8a} - 2NO_3]^{2+}$, $[\mathbf{8a} - 3NO_3]^{3+}$, and $[\mathbf{8a} - 4NO_3]^{4+}$ formed by the loss of two, three, and four NO_3^- ions, respectively. The MS (ESI) spectrum of **8c** (see Figure S39) shows peaks at m/z = 1039.00, 644.34, and 446.76 corresponding to the cations $[\mathbf{8c} - 2PF_6]^{2+}$, $[\mathbf{8c} - 3PF_6]^{3+}$, and $[\mathbf{8c} - 4PF_6]^{4+}$ formed by the loss of two, three, and four hexafluorophosphate ions, respectively. As expected on the basis of theoretical calculations, the two encapsulated Cl^- ions are retained in the formula of all these fragments. Similarly, the MS spectrum of compound **10a** (see Figure S36) displays peaks at m/z = 645.99 and 468.98 corresponding to the cations $[\mathbf{10a} - 3NO_3]^{3+}$ and $[\mathbf{10a} - 4NO_3]^{4+}$

formed by the loss of three and four NO_3^- ions, respectively. Here also, the two encapsulated Br^- ions are accounted for in the formula of the fragments. The calculated and observed isotopic distribution patterns of the peaks corresponding to the above-mentioned fragments are found to be comparable.

The exchange of the encapsulated NO_3^- with Cl^- was studied by DFT calculations using the Gaussian 09 software package[15] and the results are presented in Table S3. The calculated free energy and enthalpy for the formation of $[(Cl)_2\subset Pd_3(\mathbf{L})_4]^{4+}$ and 2 equiv. of NO_3^- from $[(NO_3)_2\subset Pd_3(\mathbf{L})_4]^{4+}$ and 2 equiv. of Cl^- were found to be –66.198 and –40.922 kcal mol^{-1}, respectively, which indicates the feasibility and exothermic nature of the anion-exchange reaction. The calculated global entropy (ΔS) is 0.084 kcal mol^{-1} K^{-1}, which indicates the spontaneous nature of the reaction.

Revisiting the Complexation of $Pd(NO_3)_2$ (Prepared from $PdCl_2$ and $AgNO_3$) with the Ligand L

So far as the nature of $Pd(NO_3)_2$ is concerned, the commercially available sample of $Pd(NO_3)_2$ provided stoichiometrically controlled revocable single discrete compounds **3a** and **4a**, but the presence of residual AgCl in the sample of $Pd(NO_3)_2$ prepared in the laboratory resulted in a mixture of products. The nature of the complexes present in the mixture could be deciphered successfully by analyzing the ^1H NMR spectra of the halide-encapsulated double-decker cages at various stages of the encapsulation process. This was possible by using the results described above for halide-encapsulated double-decker cages. The compositions of the mixtures are summarized in Table S1 in the Supporting Information.

We next considered a sample of $Pd(NO_3)_2$ prepared by the reaction of $PdCl_2$ and $AgNO_3$ in $[D_6]$DMSO with the precipitated AgCl separated by allowing the solution to stand followed by separation of the solution by using a syringe. The solution of $Pd(NO_3)_2$ thus prepared is contaminated with AgCl. For a 1:2 ratio of metal to ligand, the otherwise expected complex **3a** was found to be the major product along with good amount of **8a** and uncomplexed ligand **L** (see Scheme S20 and Figure S51). This is due to the presence of Cl^- originating from AgCl. This proposal is supported by the fact that the isolated pure complex **3a** reacts with TBACl to form **8a** and free ligand **L** (see path c of Scheme S15 and Figure S46). For a 3:4 ratio of metal to ligand, the otherwise expected complex **4a** was surprisingly found to be only a minor product, formed along with major amounts of **7a** and **8a** (see Scheme S22 and Figure S53). This has also been attributed to the presence of Cl^- originating from AgCl. This is supported by the fact that the isolated pure complex **4a** reacts with TBACl to form a mixture of **4a**, **7a**, and **8a** when a small proportion of TBACl is added and that upon increasing the amount of TBACl only **8a** results (see Scheme S8 and Figure S26). Complex **8a** is, however, stable enough if isolated; it undergoes decomplexation in the presence of excess soluble Cl^- to give the free ligand.

The deliberate addition of AgCl to **4a** also resulted in **8a**. Interestingly, the architecture of **8a** is retained even in the presence of 50 equiv. of AgCl (see Scheme S12 and Figure S41), which indicates that AgCl dissolves to an extent required for encapsulation only. Thus, **4a** could snatch Cl^- from the Ag^I ion very easily to form the more stable complex **8a**. The solubilization of AgCl in the cavities of an anion-driven interlocked cage has been reported by Clever and co-workers.[18]

Nitrate Versus Chloride: Which is a Better Template for the Double-Decker?

The complex $[Pd(\mathbf{L})_2](NO_3)_2$ (**3a**) reacted with $Pd(NO_3)_2$ to form $[(NO_3)_2\subset Pd_3(\mathbf{L})_4](NO_3)_4$ (**4a**; Scheme 2). The reaction of **3a** with a calculated amount of $Pd(NO_3)_2$ as well as TBACl resulted in the formation of $[(Cl)_2\subset Pd_3(\mathbf{L})_4](NO_3)_4$ (**8a**; Scheme 3). Complex **3a** remained unchanged upon addition of only $TBANO_3$ (see Figure S45 in the Supporting Information), whereas it underwent reorganization upon addition of only TBACl, that is, even in the absence of additional $Pd(NO_3)_2$ (see Scheme S15 and Figure S46). The products formed from the reaction of 3 equiv. of **3a** with TBACl were found to be 1 equiv. of $[(Cl)_2\subset Pd_3(\mathbf{L})_4](NO_3)_4$ (**8a**) and 2 equiv. of the free ligand **L**. Ironically, the ligand is released by the force of the templating Cl^-. Complex **4a** can be converted into **8a** upon addition of TBACl. This indicates that Cl^- is more suited as a template for the construction of the double-decker cage than NO_3^-. The presence of additional soluble NO_3^- was found to have no effect on the NO_3^--templated double-decker cage **4a** or the Cl^--templated double-decker cage **8a** in solution. However, soluble Cl^- was found to be harmful to **4a** and **8a**. Thus, NO_3^- and Cl^- are suitable for the creation of double-decker cages, with Cl^- found to be more powerful than NO_3^-. The stabilization of these cages, however, requires a suitable environment.

Decomplexation of the Double-Decker Cages

The isolated cage **8a** remained stable when redissolved in $[D_6]$DMSO, but it underwent decomplexation in the presence of an additional amount of soluble Cl^- (TBACl) to release the free ligand (Scheme 4 and Figure S47 in the Supporting Information). Thus, the decomplexation of **8a** occurs upon the addition of soluble Cl^-. Like Cl^-, soluble Br^- in excess is also harmful to the double-decker cages. The H_b protons of **8a** are shifted downfield upon addition of TBACl, whereas the other signals of **8a** are unchanged. Thus, the bowl-like exohedral space is proposed to accommodate the Cl^- ion initially and the ligand is released subsequently over a period of 12 h. In this process, the replacement of ligands by halide ions and the existence of related equilibria cannot be ruled out. However, no evidence for the intermediates formed during such exchanges could be found. The addition of TBABr to **10a** also exhibited similar behavior (see Scheme S17 and Figure S48). On addition of TBABr to **8a** and TBACl to **10a**, the signals of H_b are shifted downfield with eventual decomplexation of the cage molecules (see Figures S49 and S50). It is not very clear whether Cl^- or Br^- is the more powerful in promoting the decomplexation of the cages.

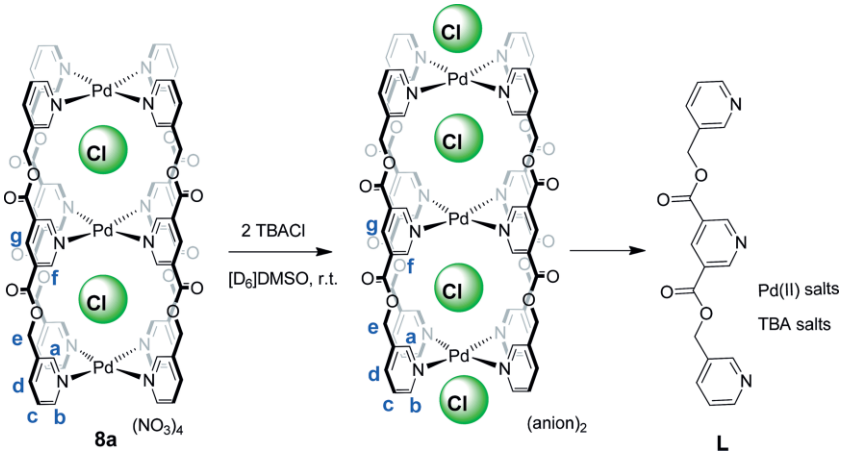

Scheme 4. Addition of 2 equiv. of TBACl to isolated $[(Cl)_2{\subset}Pd_3(L)_4](NO_3)_4$ (**8a**).

Complexation of $Pd(Y)_2$ (Prepared from PdI_2 and AgY) with the Ligand L

So far as the halide-encapsulated double-decker cages $[(X)_2{\subset}Pd_3(\mathbf{L})_4](NO_3)_4$ are concerned, NO_3^-, F^-, Cl^-, and Br^-proved suitable as guests ions, whereas I^- is unsuitable. So far as the nature of $Pd(NO_3)_2$ is concerned, the "commercially available" salt provided stoichiometrically controlled, revocable, single discrete compounds **3a** and **4a**, whereas the presence of residual Cl^- in the solution prepared in the laboratory resulted in a mixture of products. We therefore prepared $Pd(Y)_2$ from PdI_2 and AgY (Y = NO_3^-, BF_4^-, PF_6^-, $CF_3SO_3^-$, or ClO_4^-). It was confidently anticipated that the presence of residual AgI, if any, should not hamper the complexation reactions. However, the role of counter anion, Y, as a guest/template or otherwise should be reflected in this study.

The role of NO_3^- as a template for the synthesis of the $Pd_3\mathbf{L}_4$ architecture was confirmed above. A sample of $Pd(NO_3)_2$ prepared by reacting PdI_2 with $AgNO_3$ behaved very much like the commercially acquired $Pd(NO_3)_2$ (see Figures S55 and S56). The reaction of $Pd(Y)_2$ (Y = BF_4^-, PF_6^-, $CF_3SO_3^-$, or ClO_4^-) with the ligand **L** in a 1:2 ratio resulted in $[Pd(\mathbf{L})_2](Y)_2$ (**3b**–**3e**, respectively; see Scheme S28a and Figure S59). The reaction of these $Pd(Y)_2$ salts with the ligand in a 3:4 ratio also resulted in the mononuclear complexes **3b**–**3e** along with unreacted Pd^{II} salts (Scheme 5 and Figure S59). The mononuclear complexes did not reorganize to form the corresponding trinuclear complexes, even at higher temperatures, which indicates that the BF_4^-, PF_6^-, $CF_3SO_3^-$, and ClO_4^- anions are not suitable templates for the construction of double-decker cages. However, the addition of $TBANO_3$ or TBACl to **3b**–**3e** led to smooth reorganization to the corresponding NO_3^-- and Cl^--encapsulated double-decker cages $[(NO_3)_2{\subset}Pd_3(\mathbf{L})_4](Y)_4$ (**4b**–**4e**) and $[(Cl)_2{\subset}Pd_3(\mathbf{L})_4](Y)_4$ (**8b**–**8e**), respectively (see Figure S60). It is easy to conclude that the required amount of Pd^{II} ion is not a sufficient criterion for the synthesis of the double-decker cages. A suitable anion that could act as template is essential for the construction. Also, the double-decker formed in the presence of NO_3^- must encapsulate two units of the anion, as the cavities are separated, and hence the formula of **4a** would be best represented by $[(NO_3)_2{\subset}Pd_3(\mathbf{L})_4](NO_3)_4$ (**4a**). The binding of a unit of NO_3^- in the cavity of a $Pd_2\mathbf{L}_4$-type cage is a known phenomenon.[8a]

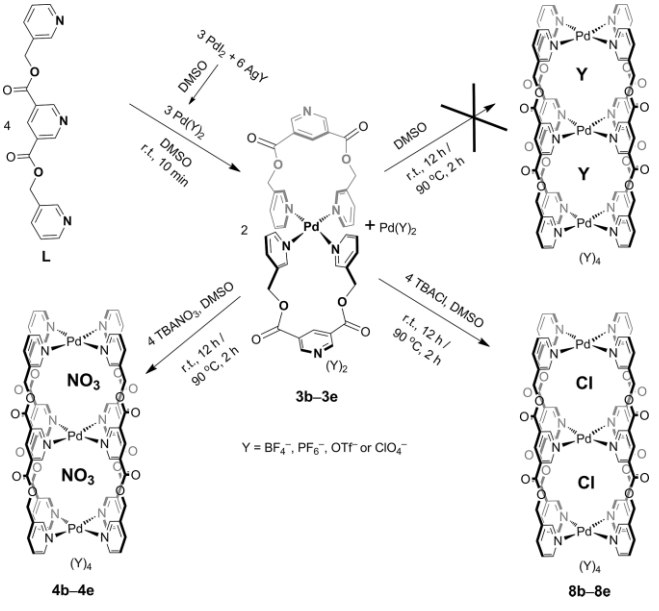

Scheme 5. Reaction of $Pd(Y)_2$ (prepared from PdI_2 and AgY, Y = BF_4^-, PF_6^-, $CF_3SO_3^-$, or ClO_4^-) and ligand **L** in a 3:4 ratio to give the mononuclear complexes $[Pd(\mathbf{L})_2](Y)_2$ (**3b**–**3e**). Upon addition of TBACl or $TBANO_3$ the trinuclear complexes $[(Cl)_2{\subset}Pd_3(\mathbf{L})_4](Y)_4$ (**8b**–**8e**) or $[(NO_3)_2{\subset}Pd_3(\mathbf{L})_4](Y)_4$ (**4b**–**4e**) are formed, respectively.

Samples of $Pd(Y)_2$ prepared from $PdCl_2$ (instead of PdI_2) and AgY will be contaminated with the Cl^- ion. The reaction of such samples of $Pd(Y)_2$ with the ligand **L** is bound to furnish a mixture of products due to the templating nature of the residual Cl^-. The reaction of $PdCl_2$ and $AgPF_6$ resulted in $Pd(PF_6)_2$, which is also contaminated with AgCl. The reaction of $Pd(PF_6)_2$ thus prepared with the ligand **L** resulted in a mixture of products (see Figures S57 and S58), with PF_6^-an innocent spectator and only the residual Cl^- influencing the complexation by favoring the formation of the double-decker structure.

Crystal Structures of $[Pd(L)_2](NO_3)_2 \cdot 2CHCl_3$ (3a·2CHCl$_3$) and $[Pd(L)_2](BF_4)_2$, (3b)

Single crystals of **3a** suitable for X-ray diffraction were grown by layering a solution of commercially acquired $Pd(NO_3)_2$ in acetonitrile over a solution of ligand **L** in chloroform. The molecular formula of the crystal structure $[Pd(\mathbf{L})_2](NO_3)_2 \cdot 2CHCl_3$ (**3a**·2CHCl$_3$) includes two $CHCl_3$ molecules as the solvent of crystallization. The coordination environment of the square-planar Pd^{II} center is occupied by two units of the ligand **L**. The ligand adopts a "U-shape" and metallo-macrocycle loops are formed to create the "spiro-type" complex $Pd_1\mathbf{L}_2$, as shown in Figure 6 (a). The two strands of each ligand are coordinated in the *cis* positions of the Pd^{II} center with one ligand loop oriented above and the other below the coordination square plane. The Pd–N bond lengths in the complex are in the range 2.027(18)–2.038(14) Å and the *cis*-N–Pd–N bond angles span the range 87.33(10)–92.67(7)°.

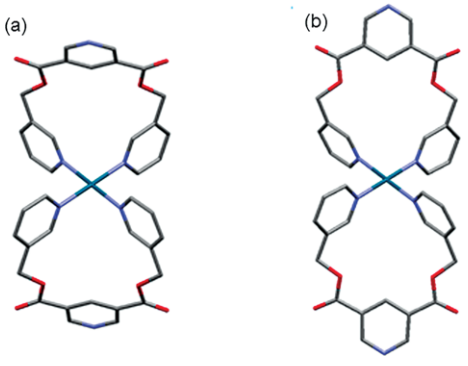

Figure 6. Crystal structures of (a) $[Pd(\mathbf{L})_2](NO_3)_2 \cdot 2CHCl_3$ (**3a**·2CHCl$_3$) and (b) $[Pd(\mathbf{L})_2](BF_4)_2$ (**3b**). The counter anions and solvent have been omitted for clarity.

A variety of solvents were diffused into samples of **3b** in DMSO in separate experiments. The diffusion of *tert*-butyl alcohol into the solution of **3b** afforded single crystals suitable for X-ray diffraction. The crystal structure confirmed the molecular structure of **3b** as shown in Figure 6 (b). The Pd–N bond lengths in the complex are in the range 2.018(3)–2.027(3) Å and the *cis*-N–Pd–N bond angles span the range 88.40(13)–91.60(12)°.

Although the basic frameworks of the complexed cations in the crystal structures of **3a**·2CHCl$_3$ and **3b** are comparable, close comparison of their structures showed a small difference in the orientation of the internal pyridine rings and an appreciable difference in their packing, as shown in Figures S64 and S65.

Crystal Structures of $[(Cl)_2 \subset Pd_3(L)_4](BF_4)_4 \cdot 2DMF$ (8b·2DMF) and $[(Cl)_2 \subset Pd_3(L)_4](PF_6)_4$ (8c)

The isolated complex **8b** was redissolved in DMF and EtOAc was diffused slowly through this solution. Single crystals suitable for X-ray diffraction were obtained over a period of 2 weeks. Single crystals of **8c** suitable for X-ray diffraction were obtained by the slow diffusion of toluene into a solution of **8c** in DMF.

The crystal structures of **8b** and **8c** are comparable (Figure 7) and therefore we will describe only the latter here. The structure of **8c** demonstrates a double-decker arrangement elaborated with two cavities, each of which accommodates one Cl^- ion; the PF_6^- ions are located outside of the cavities. The Pd–N bond lengths involving the terminal and internal pyridine nitrogen atoms span the ranges 2.013(5)–2.030(4) and 2.066(3)–2.067(4) Å, respectively. The *cis*-N–Pd–N bond angles of the two outer Pd^{II} atoms and the single inner Pd^{II} atom span the ranges 88.83(20)–91.06(19) and 88.36(15)–91.64(14)°, respectively. The Pd···Pd nonbonding distances across a given cavity and between two terminal Pd^{II} centers are 6.970(5) and 13.940(10) Å, respectively. The encapsulated Cl^- ions are in close contact with the inwardly pointing H atoms of the ligand strands (i.e., H_a and H_f, as denoted in Scheme 1 and Scheme 2) of the double-decker cage. The calculated H(py)···Cl distances span the range 2.731(10)–2.807(9) Å,[17] and are indicative of hydrogen-bonding interactions. The elaborated packing diagrams of **8b** and **8c** in three-dimensions are shown Figures S66 and S67.

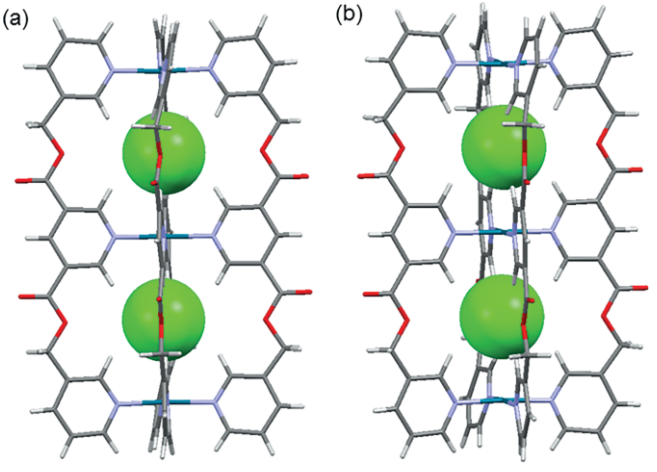

Figure 7. Crystal structures of (a) $[(Cl)_2 \subset Pd_3(\mathbf{L})\mathbf{4}](BF_4)_4 \cdot 2DMF$ (**8b**·2DMF) and (b) $[(Cl)_2 \subset Pd_3(\mathbf{L})\mathbf{4}](PF_6)_4$ (**8c**) depicting the encapsulation of chloride ions in the cavities. The counter anions outside of the cavity have been omitted for clarity.

Conclusions

We have studied the differential coordinating abilities of a tridentate ligand by using *cis*-protected or simple Pd^{II} moieties as the metal components. A subtle change in the counter anion of the metal components hugely influences the self-assembly phenomena. It is now necessary to prepare more examples of "double-decker" cages and study their nature to recognize new and emergent behavior in supramolecular coordination chemistry with particular reference to discrete, self-assembled coordination cage molecules.

Experimental Section

Ligand precursors (i.e., pyridine-3,5-dicarboxylic acid and 3-hydroxymethylpyridine), palladium salts [i.e., $PdCl_2$, PdI_2, and $Pd(NO_3)_2$], tetra-*n*-butylammonium salts (i.e., TBAF, TBACl, TBABr TBAI, and $TBANO_3$), and silver salts (i.e., $AgNO_3$, $AgBF_4$, $AgPF_6$, $AgCF_3SO_3$, and $AgClO_4$) were obtained from Sigma–Aldrich. Common reagents,

such as tmeda, NH_4PF_6, and solvents were obtained from Spectro Chem, India. The reagents were used as received unless specified otherwise. *cis*-[Pd(tmeda)Cl_2] and *cis*-[Pd(tmeda)$(NO_3)_2$] were prepared according to literature procedures.[19] The *cis*-protected Pd^{II} components, that is, *cis*-[Pd(tmeda)$(Y)_2$] (Y = NO_3^-, BF_4^-, PF_6^-, $CF_3SO_3^-$, and ClO_4^-) were prepared by the reaction of *cis*-[Pd(tmeda)Cl_2] with AgY (see Supporting Information). The deuteriated solvents $CDCl_3$ and [D_6]DMSO were obtained from Sigma–Aldrich. NMR spectra were recorded in $CDCl_3$ and [D_6]DMSO at room temperature with Bruker AV400 and AV500 spectrometers (400 and 500 MHz for ^1H NMR; 100 and 125 MHz for ^{13}C NMR). Chemical shifts are reported in ppm relative to residual solvent protons (δ = 7.26 ppm for $CDCl_3$ in ^1H NMR and δ = 77.16 ppm in ^{13}C NMR; δ = 2.50 ppm for [D_6]DMSO in ^1H NMR and δ = 39.43 ppm in ^{13}C NMR). MS (ESI) spectra were recorded with Agilent Q-TOF and Micromass Q-TOF spectrometers. Single-crystal X-ray diffraction analysis was carried out by using a Bruker APEX II-CCD XRD diffractometer. CHN analysis was performed with a Perkin–Elmer 2400 series CHNS/O Analyzer. Melting points were determined using a CINTEX apparatus.

Synthesis of the Ligand (L): A 100 mL round-bottomed flask was charged with pyridine-3,5-dicarboxylic acid (0.618 g, 3.7 mmol) and $SOCl_2$ (20 mL) and the mixture was heated at reflux under nitrogen for 48 h. The excess $SOCl_2$ was removed by distillation under reduced pressure to give a pale-yellow solid. This solid was suspended in dry dichloromethane (20 mL) and 3-hydroxymethylpyridine (0.807 g, 7.4 mmol) was added followed by the dropwise addition of triethylamine (1 mL). The suspension was then heated at reflux for 4 h, after which the suspension was cooled to room temperature. A saturated aqueous solution of sodium hydrogen carbonate (20 mL) was then added. The organic layer was separated and then evaporated to dryness under reduced pressure. The crude product was purified by silica gel column chromatography prepared by using hexane. The column was eluted with EtOAc/hexane (1:1) to remove less polar impurities. Subsequently, elution with DCM/acetone (3:7) afforded the product as a white solid (0.954 g, isolated yield 74 %) after evaporation of the solvent and drying under vacuum, m.p. 121 °C. ^1H NMR (500 MHz, $CDCl_3$): δ = 9.38 (s, 2 H, H_f), 8.86 (s, 1 H, H_g), 8.79 (s, 2 H, H_a), 8.63 (d, J = 2.0 Hz, 2 H, H_b), 7.81 (d, J = 2.0 Hz, 2 H, H_d), 7.36–7.34 (dd, J = 0.5, 0.5 Hz, 2 H, H_c), 5.43 (s, 4 H, H_e) ppm. ^{13}C NMR (125 MHz, $CDCl_3$, 300 K): δ = 164.20, 154.65, 150.15, 149.98, 138.35, 136.58, 131.00, 125.86, 123.82, 65.12 ppm. ^1H NMR (400 MHz, [D_6]DMSO): δ = 9.33 (s, 2 H, H_f), 8.72 (s, 2 H, H_a), 8.68 (s, 1 H, H_g), 8.58 (d, J = 3.2 Hz, 2 H, H_b), 7.94 (d, J = 7.6 Hz, 2 H, H_d), 7.46–7.43 (dd, J = 4.8, 4.8 Hz, 2 H, H_c), 5.46 (s, 4 H, H_e) ppm. ^{13}C NMR(100 MHz, [D_6]DMSO, 300 K): δ = 163.75, 153.79, 149.50, 149.41, 137.28, 136.16, 131.27, 125.59, 123.66, 64.70 ppm. MS (ESI): m/z = 350.11 $[M + H]^+$. $C_{19}H_{15}N_3O_4$ (349.3): calcd. C 65.32, H 4.33, N 12.03; found C 64.37, H 4.38, N 11.77.

Synthesis of the Complexes

[Pd(tmeda)(L)]$(NO_3)_2$ (1a): The ligand **L** (0.0175 g, 0.05 mmol) was added to a solution of *cis*-[Pd(tmeda)$(NO_3)_2$] (0.0173 g, 0.05 mmol) in acetonitrile (5 mL). The reaction mixture was stirred at room temperature for 1 h to obtain a clear yellow solution. The resulting solution was poured into a watch-glass and then evaporated at room temperature by allowing to stand for 6 h to obtain a yellow solid. The solid was washed with acetone (2 × 2 mL) and dried under vacuum to afford complex **1a** (0.0295 g, isolated yield 85 %), m.p. 274 °C. ^1H NMR (400 MHz, [D_6]DMSO, 300 K): δ = 9.59 (s, 2 H, H_a), 9.37 (s, 2 H, H_f), 9.31 (d, J = 5.2 Hz, 2 H, H_b), 8.83 (s, 1 H, H_g),8.17 (d, J = 8.0 Hz, 2 H, H_d), 7.79–7.76 (m, J = 6.0, 5.6 Hz, 2 H, H_c), 5.65–5.27 (dd, J = 12.4, 12.8 Hz, 4 H, H_e), 2.96 (s, 4 H, -CH_2-), 2.44 (s, 12 H, -CH_3) ppm. ^{13}C NMR (100 MHz, [D_6]DMSO, 300 K): δ = 157.97, 151.85, 150.94, 140.24, 137.13, 131.04, 127.50, 112.92, 104.33, 65.56, 62.65, 50.96, 50.73 ppm. MS (ESI): m/z = 284, [**1a**-2NO_3]$^{2+}$.

[Pd(tmeda)(L)]$(BF_4)_2$ (1b): The ligand **L** (0.0175 g, 0.05 mmol) was added to a solution of [Pd(tmeda)]$(BF_4)_2$ (0.0198 g, 0.05 mmol) in acetonitrile (5 mL). The reaction mixture was stirred at room temperature for 1 h to obtain a clear yellow solution. The resulting solution was poured into a watch-glass and subsequently evaporated at room temperature over a period of 6 h to obtain a yellow solid. The solid was washed with acetone (2 × 2 mL) and dried under vacuum to afford complex **1b** (0.0290 g, isolated yield 78 %). The ^1H NMR spectrum of compound **1b** is comparable with that of compound **1a**.

[Pd(tmeda)(L)]$(Y)_2$ (1c–1e): Complexes [Pd(tmeda)(**L**)]$(Y)_2$ (**1c**–**1e**; Y = PF_6^-, $CF_3SO_3^-$, and ClO_4^-, respectively) were prepared in a similar manner as described for **1b** using the appropriate *cis*-protected Pd^{II} component [Pd(tmeda)]$(Y)_2$ (see the Supporting Information).

[Pd$(L)_2$]$(NO_3)_2$ (3a): The ligand **L** (0.0209 g, 0.06 mmol) was added to a solution of $Pd(NO_3)_2$ (0.0069 g, 0.03 mmol) in DMSO (3 mL). The reaction mixture was stirred at room temperature for 10 min. Subsequently, the addition of ethyl acetate (10 mL) to the resulting solution led to a white solid precipitate, which was separated by centrifugation. The solid was washed with acetonitrile (2 × 2 mL) and dried under vacuum to afford complex **3a** (0.0222 g, isolated yield 80 %), m.p. 232 °C (decomp.). ^1H NMR (500 MHz, [D_6]DMSO, 300 K): δ = 9.66 (s, 4 H, H_a), 9.39 (d, J = 1.0 Hz, 4 H, H_b), 9.38 (s, 4 H, H_f), 8.86 (s, 2 H, H_g), 8.09 (d, J = 8.0 Hz, 4 H, H_d), 7.73 (dd, J = 5.0, 5.0 Hz, 4 H, H_c), 5.43 (s, 8 H, H_e) ppm. ^{13}C NMR (125 MHz, [D_6]DMSO, 300 K): δ = 162.96, 154.27, 151.20, 150.91, 140.84, 139.77, 136.16, 127.46, 125.45, 64.77 ppm. MS (ESI): m/z = 402.15 [**3a** – 2NO_3]$^{2+}$.

[Pd$(L)_2$]$(BF_4)_2$ (3b): A sample of $Pd(BF_4)_2$ was prepared in DMSO (3 mL) by stirring a mixture of PdI_2 (0.0108 g, 0.03 mmol) and $AgBF_4$ (0.0116 g, 0.06 mmol) at 90 °C for 30 min. The precipitated AgI was separated by centrifugation and the supernatant was transferred by using a syringe. The ligand **L** (0.0209 g, 0.06 mmol) was added to the solution of $Pd(BF_4)_2$ (0.0084 g, 0.03 mmol) prepared in DMSO (3 mL), and the reaction mixture was stirred at room temperature for 10 min. Subsequently, the addition of ethyl acetate (10 mL) to the resulting solution led to a white solid precipitate, which was separated by centrifugation. The solid was washed with acetonitrile (2 × 10 mL) and dried under vacuum to afford complex **3b** (0.0241 g, isolated yield 82 %). The ^1H NMR spectrum of compound **3b** is similar to that of compound **3a**.

[Pd$(L)_2$]$(Y)_2$ (3c–3e): Complexes [Pd(**L**)$_2$]$(Y)_2$ (**3c**–**3e**; Y = PF_6^-, $CF_3SO_3^-$, and ClO_4^-, respectively) were prepared in a similar manner as described for **3b** using the appropriate silver salt (see the Supporting Information).

[$(NO_3)_2$⊂$Pd_3(L)_4$]$(NO_3)_4$ (4a): The ligand **L** (0.0139 g, 0.04 mmol) was added to a solution of $Pd(NO_3)_2$ (0.0069 g, 0.03 mmol) in DMSO (3 mL). The reaction mixture was stirred at 90 °C for 2 h. Subsequently, the addition of ethyl acetate (10 mL) to the resulting solution led to a white solid precipitate, which was separated by centrifugation. The solid was washed with acetonitrile (2 × 2 mL) and dried under vacuum to afford complex **4a** (0.0462 g, isolated yield 74 %), m.p. 300 °C (decomp.). ^1H NMR (500 MHz, [D_6]DMSO, 300 K): δ = 10.63 (s, 8 H, H_f), 9.88 (s, 8 H, H_a), 9.23 (d, J = 6.0 Hz, 8 H, H_b), 8.85 (s, 4 H, H_g), 8.12 (d, J = 8.0 Hz, 8 H, H_d), 7.79–7.76 (dd, J = 6.0, 6.0 Hz, 8 H, H_c), 5.51 (s, 16 H, H_e) ppm. ^{13}C NMR (125 MHz, [D_6]DMSO, 300 K): δ = 162.47, 157.07, 151.13, 149.43, 142.97, 139.62,

135.12, 129.49, 126.98, 65.48 ppm. MS (ESI): *m/z* = 982.73 [**4a** – $2NO_3]^{2+}$, 634.35 [**4a** – $3NO_3]^{3+}$, 460.23 [**4a** – $4NO_3]^{4+}$.

[$(NO_3)_2$⊂$Pd_3(L)_4$]$(BF_4)_4$ (4b): A sample of $Pd(BF_4)_2$ in DMSO (3 mL) was prepared in same manner as described above for the synthesis of **3b**. The ligand **L** (0.0139 g, 0.04 mmol) was added to a solution of $Pd(BF_4)_2$ (0.0084 g, 0.03 mmol) in DMSO (3 mL) followed by the addition of $TBANO_3$ (0.0122 g, 0.04 mmol) at room temperature. The reaction mixture was then heated to 90 °C and stirred for 2 h. Subsequently, the addition of ethyl acetate (10 mL) to the resulting solution led to an off-white solid precipitate, which was separated by centrifugation. The solid was washed with acetonitrile (2 × 10 mL) and dried under vacuum to afford complex **4b** (0.0538 g, isolated yield 82 %). The ^{1}H NMR spectrum of complex **4b** is similar to that of compound **4a**.

[$(NO_3)_2$⊂$Pd_3(L)_4$](Y)$_4$ (4c–4e): Complexes [$(NO_3)_2$⊂Pd_3(**L**)$_4$](Y)$_4$ (**4c**–**4e**; Y = PF_6^-, $CF_3SO_3^-$, and ClO_4^-, respectively) were prepared in a similar manner as described for **4b** using the appropriate silver salt (see the Supporting Information).

[$(F)_2$⊂$Pd_3(L)_4$]$(NO_3)_4$ (6a): A solution of tetra-*n*-butylammonium fluoride (0.0313 g, 0.12 mmol) in [D_6]DMSO (0.2 mL) was added portionwise (4 × 0.05 mL) to a clear solution of compound **4a** (0.0626 g, 0.03 mmol of complex) in [D_6]DMSO (0.4 mL, in situ) at room temperature. The solution was monitored by ^{1}H NMR spectroscopy at room temperature after the addition of each portion of the guest. The final spectrum showed a single set of peaks and a downfield shift of the pyridine α- and β-H atoms (H_f: $\Delta\delta$ = 0.512 ppm; H_a: $\Delta\delta$ = 0.378 ppm; H_b: $\Delta\delta$ = 0.313 ppm) as compared with compound **4a**, which indicates the quantitative formation of compound **6a** as a single product. The NO_3^- ions present in **4a** were exchanged with two F^- ions, as is evident from the ^{1}H NMR spectroscopic data. The complex was not very stable and could not be isolated in the solid state. In solution, additional signals started to appear in the ^{1}H NMR spectrum after 1 h and finally only signals from the ligand were seen, indicating decomplexation. ^{1}H NMR (400 MHz, [D_6]DMSO, 300 K): δ = 11.13 (s, 8 H, H_f), 10.25 (s, 8 H, H_a), 9.54 (d, *J* = 5.6 Hz, 8 H, H_b), 8.92 (s, 4 H, H_g), 8.09 (d, *J* = 8.0 Hz, 8 H, H_d), 7.85–7.82 (dd, *J* = 6.4, 6.4 Hz, 8 H, H_c), 5.54 (s, 16 H, H_e) ppm. ^{13}C NMR (100 MHz, [D_6]DMSO, 300 K): δ = 162.01, 155.98, 150.37, 147.70, 142.74, 139.64, 134.98, 129.01, 126.60, 64.59 ppm.

[$(Cl)_2$⊂$Pd_3(L)_4$]$(NO_3)_4$ (8a): Complex **8a** was prepared in a similar manner as described for **6a**, but by using a solution of tetra-*n*-butylammonium chloride (0.0333 g, 0.12 mmol) in [D_6]DMSO (0.2 mL). The final spectrum showed a single set of peaks and a downfield shift of pyridine α- and β-H atoms (H_f: $\Delta\delta$ = 0.872 ppm; H_a: $\Delta\delta$ = 0.595 ppm; H_b: $\Delta\delta$ = 0.373 ppm) as compared with compound **4a**, which indicates the quantitative formation of **8a** as a single product The NO_3^- ions present in **4a** were exchanged with two Cl^- ions as is evident from the ^{1}H NMR and MS (ESI) data.

Isolation of 8a: Complex **8a**, as described above in DMSO, was isolated by the precipitation method by adding ethyl acetate (10 mL) to the reaction mixture to afford a white precipitate. The precipitate was separated by centrifugation. The solid was washed with water (2 × 2 mL) and dried under vacuum to afford complex **8a** (0.0549 g, isolated yield 90 %), m.p. 289 °C (decomp.). ^{1}H NMR (400 MHz, [D_6]DMSO, 300 K): δ = 11.50 (s, 8 H, H_f), 10.49 (s, 8 H, H_a), 9.62 (d, *J* = 5.6 Hz, 8 H, H_b), 8.91 (s, 4 H, H_g), 8.07 (d, *J* = 8.4 Hz, 8 H, H_d), 7.86–7-83 (m, *J* = 5.6, 6.0 Hz, 8 H, H_c), 5.56 (s, 16 H, H_e) ppm. ^{13}C NMR (100 MHz, [D_6]DMSO, 300 K): δ = 161.96, 156.18, 150.36, 147.69, 142.58, 138.43, 134.69, 128.65, 126.59, 64.57 ppm. MS (ESI): *m/z* = 955.67 [**8a** – $2NO_3]^{2+}$, 616.42 [**8a** – $3NO_3]^{3+}$, 446.58 [**8a** – $4NO_3]^{4+}$.

[$(Cl)_2$⊂$Pd_3(L)_4$]$(BF_4)_4$ (8b): A sample of $Pd(BF_4)_2$ in DMSO (3 mL) was prepared in the same manner as described above for the synthesis of **3b**. The ligand **L** (0.0139 g, 0.04 mmol) was added to $Pd(BF_4)_2$ (0.0084 g, 0.03 mmol) in DMSO (3 mL) and the solution was stirred at room temperature for 10 min. Then TBACl (0.0111 g, 0.04 mmol) was added, the solution was heated to 90 °C, and the reaction mixture stirred for 2 h. Subsequently, the addition of ethyl acetate (10 mL) to the resulting solution led to an off-white solid precipitate, which was separated by centrifugation. The solid was washed with acetonitrile (2 × 10 mL) and dried under vacuum to afford complex **8b** (0.0499 g, isolated yield 78 %). The ^{1}H NMR spectrum of compound **8b** is similar to that of compound **8a**.

[$(Cl)_2$⊂$Pd_3(L)_4$](Y)$_4$ (8c–8e): Complexes [$(Cl)_2$⊂Pd_3(**L**)$_4$](Y)$_4$ (**8c**–**8e**; Y = PF_6^-, $CF_3SO_3^-$, and ClO_4^-, respectively) were prepared in a similar manner as described for **8b** using the appropriate silver salt (see the Supporting Information).

We previously prepared complex **8c** in a different manner, as described below.

[$(Cl)_2$⊂$Pd_3(L)_4$]$(PF_6)_4$ (8c): A sample of NH_4PF_6 (0.0489 g, 0.3 mmol) was added to a clear solution of complex **8a** (0.0610 g, 0.03 mmol) in CH_3CN/H_2O (1:1, 5 mL). The mixture was stirred at room temperature for 12 h. The clear solution thus obtained was evaporated at room temperature by allowing to stand. The pale-green solid obtained was washed with water (2 × 2 mL) and dried under vacuum to afford complex **8c** evident from the absence of an N–O stretching band due to NO_3^- ion at 1384 cm^{-1} [0.0624 g, isolated yield 88 %; IR (KBr pellet): $\tilde{\nu}$ = 847 (P–F stretch) cm^{-1}]. The ^{1}H NMR spectrum shows a single set of peaks, comparable to the data of compound **8a**, m.p. 263 °C (decomp.). ^{1}H NMR (500 MHz, [D_6]DMSO, 300 K): δ = 11.48 (s, 8 H, H_f), 10.48 (s, 8 H, H_a), 9.56 (d, *J* = 6.0 Hz, 8 H, H_b), 8.92 (s, 4 H, H_g), 8.05 (d, *J* = 7.0 Hz, 8 H, H_d), 7.83–7.80 (dd, *J* = 6.0, 6.0 Hz, 8 H, H_c), 5.54 (s, 16 H, H_e) ppm. ^{13}C NMR (125 MHz, [D_6]DMSO, 300 K): δ = 162.71, 156.92, 151.06, 148.47, 143.43, 139.14, 135.43, 129.40, 127.32, 65.26 ppm. MS (ESI): *m/z* = 1039.00 [**8c** – $2PF_6]^{2+}$, 644.34 [**8c** – $3PF_6]^{3+}$, 446.77 [**8c** – $4PF_6]^{4+}$.

[$(Br)_2$⊂$Pd_3(L)_4$]$(NO_3)_4$ (10a): Complex **10a** was prepared in a similar manner as described for **6a** and **8a** but by using a solution of tetra-*n*-butylammonium bromide (0.0290 g, 0.09 mmol) in [D_6]DMSO (0.2 mL). The final ^{1}H NMR spectrum shows a single set of peaks and a downfield shift of the pyridine α- and β-H atoms (H_f: $\Delta\delta$ = 1.051 ppm; H_a: $\Delta\delta$ = 0.766 ppm; H_b: $\Delta\delta$ = 0.394 ppm) as compared with compound **4a**, which indicates the quantitative formation of compound **10a** as the only product. The NO_3^- ions present in **4a** were exchanged with two Br^- ions, as is evident from the ^{1}H NMR and MS (ESI) data.

Isolation of 10a: Complex **10a**, prepared as described above in DMSO, was isolated by the precipitation method by adding ethyl acetate (10 mL) to the reaction mixture to afford a white precipitate. The precipitate was separated by centrifugation. The solid was washed with water (2 × 2 mL) and dried under vacuum to afford complex **10a** (0.0560 g, isolated yield 88 %), m.p. 300 °C (decomp.). ^{1}H NMR (400 MHz, [D_6]DMSO, 300 K): δ = 11.68 (s, 8 H, H_f), 10.65 (s, 8 H, H_a), 9.59 (d, *J* = 4.8 Hz, 8 H, H_b), 8.91 (s, 4 H, H_g), 8.09 (d, *J* = 7.2 Hz, 8 H, H_d), 7.84–7.83 (dd, *J* = 6.8, 6.8 Hz, 8 H, H_c), 5.57 (s, 16 H, H_e) ppm. ^{13}C NMR (100 MHz, [D_6]DMSO, 300 K): δ = 162.03, 156.76, 150.94, 148.43, 142.50, 138.41, 134.32, 128.52, 126.36, 64.88 ppm. MS (ESI): *m/z* = 645.99 [**10a** – $3NO_3]^{3+}$, 468.98 [**10a** – $4NO_3]^{4+}$.

CCDC 1446609 (for **1a**), 997082 (for **3a**), 1446610 (for **3b**), 1446611 (for **8b**), and 997083 (for **8c**) contain the supplementary crystallo-

graphic data for this paper. These data can be obtained free of charge from The Cambridge Crystallographic Data Centre.

Acknowledgments

D. K. C. thanks the Science and Engineering Research Board, India (SERB), Department of Science and Technology, Government of India (project number SB/S1/IC-05/2014) for financial support. We are grateful to Mr. V. Ramkumar for collecting single-crystal X-ray diffraction data. S. B. and S. S. thank the University Grants Commission (UGC), New Delhi and the Council of Scientific and Industrial Research (CSIR), New Delhi, respectively, for research fellowships. G. S. H thanks Department of Foreign Affairs and International Trade (DFAIT), Canada, Natural Sciences and Engineering Research Council of Canada (NSERC) and the University of Montreal, Canada for financial support.

Keywords: Template synthesis · Self-assembly · Palladium · Anions

[1] G. M. Whitesides, B. Grzybowski, *Science* **2002**, *295*, 2418–2421.
[2] a) H. Dasary, R. Jagan, D. K. Chand, *Chem. Eur. J.* **2015**, *21*, 1499–1507; b) M. C. Naranthatta, V. Ramkumar, D. K. Chand, *J. Chem. Sci.* **2015**, *127*, 273–280; c) S. Ganta, D. K. Chand, *Dalton Trans.* **2015**, *44*, 15181–15188; d) S. Prusty, S. Krishnaswamy, S. Bandi, B. Chandrika, J. Luo, J. S. McIndoe, G. S. Hanan, D. K. Chand, *Chem. Eur. J.* **2015**, *21*, 15174–15187.
[3] N. B. Debata, D. Tripathy, D. K. Chand, *Coord. Chem. Rev.* **2012**, *256*, 1831–1945.
[4] a) S. Mukherjee, P. S. Mukherjee, *Chem. Commun.* **2014**, *50*, 2239–2248; b) A. Mishra, R. Gupta, *Dalton Trans.* **2014**, *43*, 7668–7682; c) T. R. Cook, P. J. Stang, *Chem. Rev.* **2015**, *115*, 7001–7045.
[5] a) Q.-F. Sun, J. Iwasa, D. Ogawa, Y. Ishido, S. Sato, T. Ozeki, Y. Sei, K. Yamaguchi, M. Fujita, *Science* **2010**, *328*, 1144–1147; b) J. D. Brodin, J. R. Carr, P. A. Sontz, F. A. Tezcan, *Proc. Natl. Acad. Sci. USA* **2014**, *111*, 2897–2902; c) E. Mattia, S. Otto, *Nature Nanotechnol.* **2015**, *10*, 111–119.
[6] S. Bandi, A. K. Pal, G. S. Hanan, D. K. Chand, *Chem. Eur. J.* **2014**, *20*, 13122–13126.
[7] D. A. McMorran, P. J. Steel, *Angew. Chem. Int. Ed.* **1998**, *37*, 3295–3297; *Angew. Chem.* **1998**, *110*, 3495.
[8] a) D. K. Chand, K. Biradha, M. Fujita, *Chem. Commun.* **2001**, 1652–1653; b) H. S. Sahoo, D. K. Chand, *Dalton Trans.* **2010**, *39*, 7223–7225; c) C. Gütz, R. Hovorka, G. Schnakenburg, A. Lützen, *Chem. Eur. J.* **2013**, *19*, 10890–10894; d) D. Preston, A. Fox-Charles, W. K. C. Lo, J. D. Crowley, *Chem. Commun.* **2015**, *51*, 9042–9045; e) M. Yamashita, T. Yuki, Y. Sei, M. Akita, M. Yoshizawa, *Chem. Eur. J.* **2015**, *21*, 4200–4204.
[9] a) M. Yoshizawa, J. K. Klosterman, *Chem. Soc. Rev.* **2014**, *43*, 1885–1895; b) M. Han, D. M. Engelhard, G. H. Clever, *Chem. Soc. Rev.* **2014**, *43*, 1848–1860.
[10] D. A. McMorran, P. J. Steel, *Supramol. Chem.* **2002**, *14*, 79–85.
[11] M. D. Johnstone, E. K. Schwarze, G. H. Clever, F. M. Pfeffer, *Chem. Eur. J.* **2015**, *21*, 3948–3955.
[12] Q.-F. Sun, S. Sato, M. Fujita, *Nature Chem.* **2012**, *4*, 330–333.
[13] a) R. Maity, H. Koppetz, A. Hepp, F. E. Hahn, *J. Am. Chem. Soc.* **2013**, *135*, 4966–4969; b) L. Zhang, Y.-J. Lin, Z.-H. Li, G.-X. Jin, *J. Am. Chem. Soc.* **2015**, *137*, 13670–13678.
[14] H. S. Sahoo, D. Tripathy, S. Chakrabortty, S. Bhat, A. Kumbhar, D. K. Chand, *Inorg. Chim. Acta* **2013**, *400*, 42–50.
[15] M. J. Frisch, G. W. Trucks, H. B. Schlegel, G. E. Scuseria, M. A. Robb, J. R. Cheeseman, G. Scalmani, V. Barone, B. Mennucci, G. A. Petersson, H. Nakatsuji, M. Caricato, X. Li, H. P. Hratchian, A. F. Izmaylov, J. Bloino, G. Zheng, J. L. Sonnenberg, M. Hada, M. Ehara, K. Toyota, R. Fukuda, J. Hasegawa, M. Ishida, T. Nakajima, Y. Honda, O. Kitao, H. Nakai, T. Vreven, J. A. Montgomery Jr., J. E. Peralta, F. Ogliaro, M. Bearpark, J. J. Heyd, E. Brothers, K. N. Kudin, V. N. Staroverov, R. Kobayashi, J. Normand, K. Raghavachari, A. Rendell, J. C. Burant, S. S. Iyengar, J. Tomasi, M. Cossi, N. Rega, J. M. Millam, M. Klene, J. E. Knox, J. B. Cross, V. Bakken, C. Adamo, J. Jaramillo, R. Gomperts, R. E. Stratmann, O. Yazyev, A. J. Austin, R. Cammi, C. Pomelli, J. W. Ochterski, R. L. Martin, K. Morokuma, V. G. Zakrzewski, G. A. Voth, P. Salvador, J. J. Dannenberg, S. Dapprich, A. D. Daniels, Ö. Farkas, J. B. Foresman, J. V. Ortiz, J. Cioslowski, D. J. Fox, *Gaussian 09*, revision A.02, Gaussian, Inc., Wallingford, CT, **2009**.
[16] a) M. C. Naranthatta, D. Das, D. Tripathy, H. S. Sahoo, V. Ramkumar, D. K. Chand, *Cryst. Growth Des.* **2012**, *12*, 6012–6022; b) D. Tripathy, V. Ramkumar, D. K. Chand, *Cryst. Growth Des.* **2013**, *13*, 3763–3772; c) M. C. Naranthatta, V. Ramkumar, D. K. Chand, *J. Chem. Sci.* **2014**, *126*, 1493–1499.
[17] N. L. S. Yue, D. J. Eisler, M. C. Jennings, R. J. Puddephatt, *Inorg. Chem. Commun.* **2005**, *8*, 31–33.
[18] S. Freye, D. M. Engelhard, M. John, G. H. Clever, *Chem. Eur. J.* **2013**, *19*, 2114–2121.
[19] a) H. D. K. Drew, F. W. Pinkard, G. H. Preston, W. Wardlaw, *J. Chem. Soc.* **1932**, 1895–1909; b) S. Bandi, N. B. Debata, V. Ramkumar, D. K. Chand, *Inorg. Chem. Commun.* **2014**, *39*, 75–78.

Received: March 8, 2016
Published Online: April 24, 2016